

# Visible-Infrared Person Re-Identification via Patch-Mixed Cross-Modality Learning

Zhihao Qian<sup>1</sup>, Yutian Lin<sup>2</sup>, Bo Du<sup>3\*</sup>

<sup>1,2,3\*</sup>School of Computer Science, Wuhan University, China

## Abstract

Visible-infrared person re-identification (VI-ReID) aims to retrieve images of the same pedestrian from different modalities, where the challenges lie in the significant modality discrepancy. To alleviate the modality gap, recent methods generate intermediate images by GANs, grayscaling, or mixup strategies. However, these methods could introduce extra noise, and the semantic correspondence between the two modalities is not well learned. In this paper, we propose a Patch-Mixed Cross-Modality framework (PMCM), where two images of the same person from two modalities are split into patches and stitched into a new one for model learning. In this way, the model learns to recognize a person through patches of different styles, and the modality semantic correspondence is directly embodied. With the flexible image generation strategy, the patch-mixed images freely adjust the ratio of different modality patches, which could further alleviate the modality imbalance problem. In addition, the relationship between identity centers among modalities is explored to further reduce the modality variance, and the global-to-part constraint is introduced to regularize representation learning of part features. On two VI-ReID datasets, we report new state-of-the-art performance with the proposed method.

## 1 Introduction

Visible-infrared person re-identification (VI-ReID) [Wu *et al.*, 2017a] aims to match a target person between the RGB visible cameras and low-light infrared (IR) cameras. The task is increasing research interests [Ye *et al.*, 2018b; Ye *et al.*, 2020b; Wu *et al.*, 2021; Ling *et al.*, 2020; Huang *et al.*, 2022; Wei *et al.*, 2021] because of its great value in the practical 24-hour surveillance system. The main challenge of VI-ReID is modality discrepancy, where different wavelengths bring significantly different visual appearances (*e.g.*, color, texture).

Typically, there are three main types of methods: 1) the representation learning based methods [Lu *et al.*, 2020; Park *et al.*, 2021; Wu *et al.*, 2021], where networks are designed to learn discriminative features in a modality-shared space;

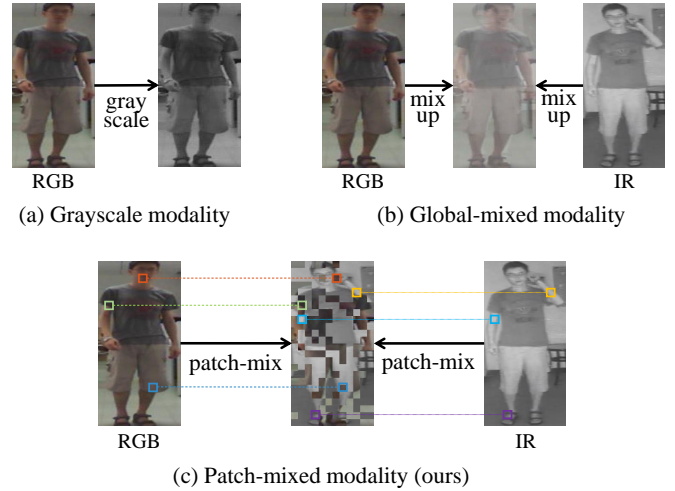


Figure 1: Different methods of generating the intermediate modality. (a) grayscale images are generated by visible images, (b) a mixed image is a global mixture of corresponding RGB and IR images, and (c) our proposed patch-mixed image which involves no additional noise, semantically corresponds between the two modalities and relieves the modality imbalance problem.

2) the metric learning based methods [Ye *et al.*, 2018b], where loss functions are designed to bridge the modality gap; 3) the modality-transform based methods [Dai *et al.*, 2018; Zhang *et al.*, 2021], which transform modalities into each other for style consistency. However, these methods try to handle the large modality discrepancy directly, while it is hard to align heterogeneous modalities without considering the correspondence between IR and RGB images.

To handle the above issue, recent works generate a third modality to assist cross-modality learning. Among them, a branch of works constructs the new modality upon only one modality. For example, [Li *et al.*, 2020] generates the third auxiliary modality by transforming the visible images to one-channel images and then reconstructs three-channel images. In [Ye *et al.*, 2020c], grayscale images are generated by visible images and are utilized to enhance the robustness against color variations. However, as shown in Fig. 1 (a), these new images are generated through only one modality, and could involve extra noise. Another branch of works [Huang *et al.*,

2022; Wei *et al.*, 2021] adopts mixup [Zhang *et al.*, 2017] strategy to generate intermediate modality images between RGB and infrared images, achieving promising results. However, as shown in Fig. 1 (b), the mixed image is neither Rgb nor IR, which may improve the generalization ability but the semantic correspondence between the two modalities is absent.

In this paper, we propose a Patch-Mixed Cross-Modality framework (PMCM), which leverages modality discrepancy by learning with a new patch-mixed modality. As shown in Fig. 1 (c), the patch-mixed image is generated by blending a person’s image of two modalities in the patch-level without involving additional noise. The patch-mixed modality benefits cross-modality learning in two aspects: 1) The semantic correspondence between two modalities could be learned by recognizing a patch-mixed image. For example, the network will be learned that the hair in the IR patch and the face in the RGB patch together describe a person’s appearance. Thereby, the model learns to deal with the two modalities in the same way, and the modality gap is reduced. 2) The patch-mixed modality also relieves the modality imbalance problem. As there usually are more images captured by daytime cameras, the data of IR and RGB images are unbalanced. With the flexible image generation approach, the proportion of different modalities can be adjusted freely to produce images with more IR information or RGB information. Therefore, the distribution of training samples is modified, which achieves an effect similar to over-sampling. To deal with the intermediate modality, we align its prediction logits to the original modalities.

As a minor contribution, we enhance the learning of modality-invariant representations by aligning cross-modality identity centers. Specifically, the distances between the identity centers among the three modalities are minimized, which directly reduces the modality gap. Besides, to regularize representation learning of part features, we take full advantage of the association between the part features and the global feature. A part alignment loss is proposed to constrain the consistency of part and global prediction distributions. With the part-based learning strategy, the discriminative part features are explored, which benefits the global feature learning in return.

The main contributions of our work can be summarized as follows:

- We propose a novel patch-mixed cross-modality learning framework for the VI-ReID task, which effectively encourages the model to treat the RGB and IR images in the same way, and alleviate the modality imbalance problem.
- We consider both inter- and intra-modality variances to further enhance the learned model. In particular, a center-to-center loss is proposed to align the identity center across modalities. A part-alignment loss is proposed to constrain the consistency of part and global prediction distributions for more discriminative representation.
- Experimental results show that our method outperforms other methods on two VI-ReID datasets by a large mar-

gin, and the data imbalance problem is effectively alleviated.

## 2 Related Work

### 2.1 Visible-Infrared Person Re-identification

VI-ReID aims to match persons of different modalities, which faces the challenge of large intra-modality variation and inter-modality discrepancy. Wu *et al.* [Wu *et al.*, 2017a] were the first to define the task, which proposed a deep zero-padding method along with a large-scale VI-ReID dataset named SYSU-MM01.

Following that, researchers propose to learn modality-specific and modality-shared feature representations by designing networks or loss functions. Ye *et al.* [Ye *et al.*, 2018a] jointly optimize the modality-specific and modality-shared metrics with a hierarchical learning framework.

Lu *et al.* [Lu *et al.*, 2020] design a sharable-specific feature transfer network to complement features of one modality with specific features of the other modality. Ling *et al.* [Ling *et al.*, 2021] propose a Multi-Constraint similarity learning method that jointly considers the cross-modality relationships from three different aspects. Sun *et al.* [Sun *et al.*, 2022] performs pixel-to-pixel dense alignment acting on the intermediate representations.

On the other hand, another branch of works aims to bridge the modality discrepancy by transforming the images from one modality to the other by generative adversarial networks (GANs). For example, Dai *et al.* [Dai *et al.*, 2018] and Wang *et al.* [Ye *et al.*, 2020b] both design a cross-modality GAN to transform the two modalities to each other to learn modality-invariant feature representations. Choi *et al.* [Choi *et al.*, 2020] propose an effective generator to extract pose-invariant and illumination-invariant features. Wang *et al.* [Wang *et al.*, 2019a] transform RGB images into IR versions in pixel-level and align real and fake IR images in feature-level. Zhao *et al.* [Zhao *et al.*, 2021] learns the color-irrelevant features and aligns the identity-level feature distributions. Zhang *et al.* [Zhang *et al.*, 2022] compensate for the missing modality-specific information from the other modality in feature-level.

### 2.2 VI-ReID with Intermediate Modality Images

To further reduce the modality gap, researchers propose to construct a third modality to assist shared feature space learning. In [Li *et al.*, 2020], a third auxiliary modality is generated by transforming the visible images to one-channel images and then reconstructing three-channel images. In [Ye *et al.*, 2020c], grayscale images are generated by visible images and are utilized to enhance the robustness against color variations. Following that, [Zhang *et al.*, 2021] transforms both of the two modalities into the grayscale for modality alignment to reduce the modality discrepancy. However, in these methods, the third modality is generated upon only one modality, without considering the relationship between IR and RGB images.

Recently, some methods propose to generate intermediate modality images between RGB and infrared images, which achieve promising results. In [Ling *et al.*, 2020], inspired

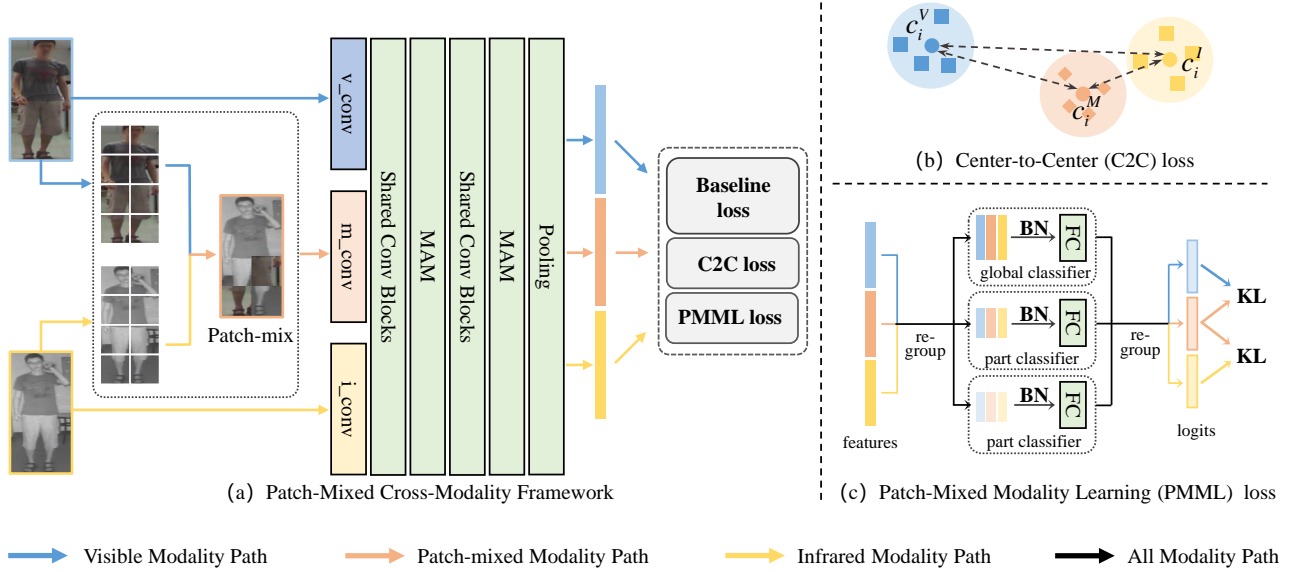


Figure 2: (a) Framework of the proposed PMCM. The patch-mixed image and the original images are together fed into the backbone network to extract features. After pooling, the obtained features are jointly optimized by the baseline loss, center-to-center loss, and patch-mixed modality learning loss. (b) Center-to-center (C2C) loss attempts to reduce the distance between the identity centers of any two modalities. (c) Patch-Mixed Modality Learning (PMML) loss aims to align the prediction distributions of the patch-mixed modality with that of the other two modalities, where global and local features are considered.

by mixup [Zhang *et al.*, 2017], a linear interpolation is performed of two images from different modalities for the same identities to generate mixed images. Similarly, in [Huang *et al.*, 2022], mixed modality images are generated with a dynamic mixup ratio learned by a deep reinforcement learning framework. In [Wei *et al.*, 2021], a syncretic modality collaborative learning model is designed, where shallow representation is mixed.

### 2.3 Modality Imbalanced Learning

Current research on imbalanced data focuses on the class imbalance problem and introduces two main strategies: re-sampling and re-weighting. Re-sampling like [Cui *et al.*, 2019; Huang *et al.*, 2016] over-sample classes with few samples and under-sample classes with many samples. Re-weighting like [Cao *et al.*, 2019; Shen *et al.*, 2016] adaptively adjusts the weights of different classes in the loss function. Liu *et al.* [Liu *et al.*, 2022a] first notice the unique data imbalance problem in cross-modality tasks and name it Modality Imbalance, which refers to the situation that one modality contains more samples than the other modality. To address the problem, they borrow the idea of re-weighting and allow independent augmentation for a specified modality. Different from their work, our PMCM alleviates this problem by adjusting the ratio of patch-mix, where more patches of one modality can be contained for data balance.

## 3 Proposed Method

In this paper, we aim to learn modality-invariant representations by an intermediate patch-mixed modality, where cross-modality retrieval can be achieved. The overview of the proposed method is shown in Fig. 2, where RGB, IR and patch-

mixed images are fed into the network, optimized by the baseline losses, center-to-center loss, and the patch-mixed modality learning loss.

Following, we introduce our method in detail. We begin with the baseline method for this task. Then we illustrate the modality center alignment and patch-mixed cross-modality framework.

### 3.1 Baseline method

We adopt a two-stream network as our baseline and sample the same number of RGB and IR images in a mini-batch. We introduce the ResNet-50 as the backbone, where the first convolution blocks are modality-unique in order to learn modality-invariant low-level features, and the others are weight-shared to capture discriminative features. Besides, we alter channel-wise attention to part-wise attention in MAMs proposed by Wu *et al.* [Wu *et al.*, 2021] and insert them into the backbone to extract modality-irrelevant feature maps. After the backbone, we only adopt global average pooling to the obtained feature maps to attain global features and then use a batch normalization layer to get the query representations. At last, the loss function for the baseline is formulated as follows:

$$\mathcal{L}_{base\_global} = \mathcal{L}_{id,g} + \mathcal{L}_{tri} + \lambda_1 \mathcal{L}_{s2s,g}, \quad (1)$$

where  $\mathcal{L}_{id,g}$  is the cross-entropy loss of the global features,  $\mathcal{L}_{tri}$  is the hard triplet loss [Hermans *et al.*, 2017],  $\lambda_1$  denotes the weight of  $\mathcal{L}_{s2s,g}$ , which is the sample-to-sample loss [Zhang *et al.*, 2021], attempting to pull close the sample features of different modalities with the same identity. Specifically, given the global features of two modalities, RGB and

IR, the sample-to-sample loss is formulated as:

$$\mathcal{L}_{s2s} = \frac{1}{N} \sum_{i=1}^N \text{mean}[F(f_i^V) - F(f_i^I)], \quad (2)$$

where  $N$  is the number of paired samples in a mini-batch,  $f_i^V$  and  $f_i^I$  are the feature of the  $i$ -th sample of RGB and IR, respectively.  $F(\cdot)$  is a network with two fully-connected layers.

**Baseline with part-based learning.** Inspired by PCB [Sun *et al.*, 2018], recent VI-ReID works [Zhang *et al.*, 2021; Zhao *et al.*, 2021; Wu *et al.*, 2021] learn part-based features to enhance global discriminative representation learning and achieve promising performance. In this work, we also exploit horizontal stripes to obtain part features. Similarly, cross-entropy loss and sample-to-sample loss are adopted to address the part-based features:

$$\mathcal{L}_{\text{base-part}} = \mathcal{L}_{\text{id},p} + \lambda_1 \mathcal{L}_{s2s,p}. \quad (3)$$

In addition, since the global and part feature both describe the same identity, we hope that the output distribution of part features could be similar to the global feature. Therefore, we calculate the KL divergence of the two output distributions as the regularization term, to learn more generalized part features. Given part and global features, the part alignment loss can be formulated as:

$$\mathcal{L}_{\text{part-align}} = \sum_{i=1}^N \sum_{k=1}^P C_g(f_i^g) \log \frac{C_g(f_i^g)}{C_{p_k}(f_i^{p_k})}, \quad (4)$$

where  $P$  is the number of parts,  $f_i^{p_k}$  denotes the feature of the  $k$ -th part feature of the  $i$ -th identity,  $C_g(\cdot)$  and  $C_{p_k}(\cdot)$  are the classifier of global features and that of the  $k$ -th part features.

Besides, in order to speed up the convergence of the model, we reduce the weight of losses involving part features in the early stage of training, which may cause relatively large interference. Therefore we set a weight  $\mu$  to losses involving part features, which linearly increases with epochs. In this way, the total loss of the part-based baseline is formulated as follows:

$$\mathcal{L}_{\text{base}} = \mathcal{L}_{\text{base-global}} + \mu(\mathcal{L}_{\text{base-part}} + \mathcal{L}_{\text{part-align}}). \quad (5)$$

### 3.2 Modality Center Alignment

To further reduce the cross-modality variance, we consider directly aligning the identity centers between any two modalities. We propose a novel center-to-center loss, where the distance between each center of the same identity from different modalities is minimized as shown in Fig. 2(b). The center of an identity  $i$  is calculated as:

$$c_i = \frac{1}{N} \sum_{i=1}^N f_i, \quad (6)$$

where  $N$  is the number of samples in the corresponding modality. Then Given the global features of RGB images and IR images, the center-to-center loss is defined as:

$$\mathcal{L}_{c2c}^g = \frac{1}{K} \sum_{i=1}^K \|c_i^V - c_i^I\|^2, \quad (7)$$

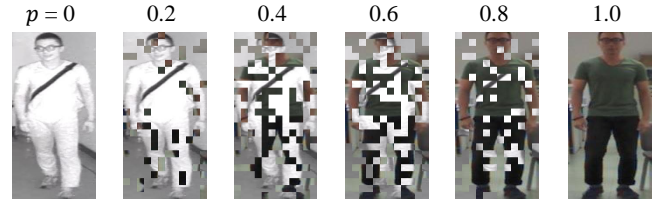


Figure 3: Patch-mixed images with different mix ratios  $p$ . When  $p = 0$ , the image is composed of only an infrared image. As  $p$  increases, more visible patches are adopted.

where  $c_i^{V,g}$  and  $c_i^{I,g}$  denote the center of the  $i$ -th identity in the RGB and IR modality, respectively.  $K$  is the number of identities. Similarly, we consider the center relations between part features and use  $\mu$  to balance the global and part losses. The final center-to-center loss is calculated as:

$$\mathcal{L}_{c2c} = \lambda_2 \mathcal{L}_{c2c,g} + \mu \lambda_3 \mathcal{L}_{c2c,p} \quad (8)$$

where  $\lambda_2$  and  $\lambda_3$  are the weights of  $\mathcal{L}_{c2c,g}$  and  $\mathcal{L}_{c2c,p}$ .

In practice, we adopt a memory bank to record the features to calculate identity centers, where the memory bank is updated along with training. Since the stored features in the memory are inconsistent with that trained in the current training batch, we set a threshold epoch to delay the optimization of this loss until the model gets stable.

### 3.3 Patch-Mixed Cross-Modality Learning

To deal with the modality variance, recent VI-ReID works [Ye *et al.*, 2020c; Huang *et al.*, 2022; Ling *et al.*, 2020] construct intermediate modalities and achieve promising performance. Different from these grayscale or mixup-based methods, we propose a novel patch-mixed intermediate modality, where each patch is from the original IR and RGB images without the extra noise.

Given an infrared image  $x^I$  and a visible image  $x^V$ , a patch-mixed image  $x^M$  is generated, where each patch  $x^M(i, j)$  is formed by either  $x^V(i, j)$  or  $x^I(i, j)$ . Here,  $i$  and  $j$  denote the patch index of image length and width, respectively. We set the probability of choosing an RGB patch to be  $p$ , then the probability of choosing an infrared patch is  $1 - p$ . As shown in Fig. 3, the ratio  $p$  balances the information from two modalities.

The patch mixed images encourage cross-modality learning from two aspects. First, the semantic information from two modalities is aligned, where the model learns to recognize the same semantic part through different modality patches. Therefore, the modality variance is bridged and the generalization ability is improved. Second, the patch-mixed images help to reduce the modality imbalance. Usually, images captured by daytime cameras are more than that of nighttime cameras, so the data of IR and RGB images are typically unbalanced. As shown in Fig. 3, with an adjustable ratio  $p$ , images with more IR information or RGB information can be generated freely according to the data distribution.

**Patch-Mixed Modality Learning (PMML).** Considering that the mixed modality contains internal information in both of the two modalities, we align it with the other two modalities.

Table 1: Comparison of CMC and mAP performances with the SOTAs on **SYSU-MM01**. Particularly, methods in the last four lines adopt different strategies to generate a intermediate modality for model learning.

Method	Pub.	All-search								Indoor-Search							
		Single-Shot				Multi-Shot				Single-Shot				Multi-Shot			
		R1	R10	R20	mAP	R1	R10	R20	mAP	R1	R10	R20	mAP	R1	R10	R20	mAP
Zero-Padding	ICCV17	14.80	54.12	71.33	15.95	19.13	61.40	78.41	10.89	20.58	68.38	85.79	26.92	24.43	75.86	91.32	18.64
cmGAN	IJCAI18	26.97	67.51	80.56	27.80	31.49	72.74	85.01	22.27	31.63	77.23	89.18	42.19	37.00	80.94	92.11	32.76
D <sup>2</sup> RL	CVPR19	28.90	70.60	82.40	29.20	-	-	-	-	-	-	-	-	-	-	-	-
AlignGAN	ICCV19	42.40	85.00	93.70	40.70	51.50	89.40	95.70	33.90	45.90	87.60	94.40	54.30	57.10	92.70	97.40	45.30
Hi-CMD	CVPR20	34.94	77.58	-	35.94	-	-	-	-	-	-	-	-	-	-	-	-
cm-SSFT	CVPR20	61.60	89.20	93.90	63.20	63.40	91.20	95.70	62.00	70.50	94.90	97.70	72.60	73.00	96.30	99.10	72.40
DDAG	ECCV20	54.75	90.39	95.81	53.02	-	-	-	-	61.02	94.06	98.41	67.98	-	-	-	-
X-Modality	AAAI20	49.92	89.79	95.96	50.73	-	-	-	-	-	-	-	-	-	-	-	-
MMN	MM21	70.6	96.2	99.0	66.9	-	-	-	-	76.2	97.2	99.3	79.6	-	-	-	-
LbA	ICCV21	54.14	-	-	55.41	-	-	-	-	66.33	-	-	58.46	-	-	-	-
MSA	IJCAI21	63.13	-	-	59.22	-	-	-	-	67.18	-	-	72.74	-	-	-	-
JCCL	AAAI21	57.20	94.30	98.40	59.30	60.70	95.20	98.60	52.60	66.60	98.80	99.70	74.70	73.80	99.40	99.90	68.30
DCLNet	MM22	70.79	-	-	65.18	-	-	-	-	73.51	-	-	76.80	-	-	-	-
FMCNet	CVPR22	66.34	-	-	62.51	73.44	-	-	56.06	68.15	-	-	74.09	78.86	-	-	63.82
MPANet	CVPR21	<b>70.58</b>	<b>96.21</b>	<b>98.80</b>	<b>68.24</b>	<b>75.58</b>	<b>97.91</b>	<b>99.43</b>	<b>62.91</b>	<b>76.74</b>	<b>98.21</b>	<b>99.57</b>	<b>80.95</b>	<b>84.22</b>	<b>99.66</b>	<b>99.96</b>	<b>75.11</b>
MAUM	CVPR22	<b>71.68</b>	-	-	<b>68.79</b>	-	-	-	-	<b>76.97</b>	-	-	<b>81.94</b>	-	-	-	-
CMM	MM20	51.80	92.72	97.71	51.21	56.27	94.08	98.12	43.39	54.98	94.38	99.41	63.7	60.42	96.88	99.5	53.52
SMCL	ICCV21	67.39	92.87	96.76	61.78	72.15	90.66	94.32	54.93	68.84	96.55	98.77	75.56	79.57	95.33	98.00	66.57
MID	AAAI22	60.27	92.90	-	59.40	-	-	-	-	64.86	96.12	-	70.12	-	-	-	-
PMCM(ours)	-	<b>75.54</b>	<b>97.49</b>	<b>99.30</b>	<b>71.16</b>	<b>82.52</b>	<b>99.00</b>	<b>99.78</b>	<b>65.88</b>	<b>81.52</b>	<b>98.99</b>	<b>99.71</b>	<b>84.33</b>	<b>90.06</b>	<b>99.80</b>	<b>99.97</b>	<b>79.45</b>
$\Delta$	-	3.86	1.28	0.50	2.37	6.94	1.09	0.25	2.97	4.55	0.78	0.14	2.39	5.84	0.14	0.01	4.34

As shown in Fig. 2 (c), we input three training samples in three modalities with the same identity into the network and obtain their output distribution. The KL divergence of the two output distributions is calculated to constrain the learning of patch-mixed modality. Since the logits are grouped by global and part relationship after the classifiers, we first regroup the logits by modality, and then align between the mixed modality and the two original modalities.

Given part and global features, the part alignment loss can be formulated as:

$$\begin{aligned} \mathcal{L}_{pmml}^{M,V} = & \sum_{i=1}^N C_g(f_i^{V,g}) \log \frac{C_g(f_i^{V,g})}{C_{p_k}(f_i^{M,g})} \\ & + \sum_{i=1}^N \sum_{k=1}^P C_{p_k}(f_i^{V,p_k}) \log \frac{C_{p_k}(f_i^{V,p_k})}{C_{p_k}(f_i^{M,p_k})} \end{aligned} \quad (9)$$

where  $f_i^{p_k}$  denotes the feature of the  $k$ -th part feature of the  $i$ -th identity,  $C_g(\cdot)$  and  $C_{p_k}(\cdot)$  are the classifier of global features and that of the  $k$ -th part features.

Similarly, the alignment between the patch-mixed images and infrared images is calculated. The total patch-mixed modality learning loss is defined as:

$$\mathcal{L}_{pmml} = p\mathcal{L}_{pmml}^{M,V} + (1-p)\mathcal{L}_{pmml}^{M,I}. \quad (10)$$

Note that to further alleviate the modality imbalance problem, we adopt a weight  $p$  to balance the two losses, which is the same as the ratio of patch-mix. The effect of ratio  $p$  is that the more image information of one modality the mixed modality contains, the more similar it will be to the source modality.

### 3.4 Optimization

We optimize the PMCM in an end-to-end manner with the final loss defined as follows:

$$\mathcal{L} = \mathcal{L}_{base} + \mathcal{L}_{c2c} + \mu\mathcal{L}_{pmml} \quad (11)$$

## 4 Experiments

### 4.1 Experimental Settings

**Datasets.** We evaluate our proposed framework on two VI-ReID datasets, SYSU-MM01 [Wu *et al.*, 2017b] and RegDB [Nguyen *et al.*, 2017].

The SYSU-MM01 dataset contains 491 identities captured by 4 visible cameras and 2 infrared cameras both including indoor and outdoor environments. The training set contains 22258 visible images and 11909 infrared images involving 395 identities, while the testing set contains 96 identities with 3803 infrared images as query images. Following the protocols, we test it both in all-search mode and indoor-search mode for only single-shot.

The RegDB dataset contains 412 identities with 206 identities for training and 206 identities for testing, where each identity has 10 visible images and 10 infrared images from a pair of overlapping visible and infrared cameras. Following the protocols, we test it both in Visible2Thermal mode, where visible images as query and infrared images as the gallery, and Thermal2Visible mode similar to the former.

**Evaluation metrics.** For both datasets, we adopt the Cumulative Matching Characteristic (CMC) and mean Average Precision (mAP) to evaluate the performance and take the average result of ten tests to report.

**Implementation details.** We implement our method with PyTorch and use ResNet50 pre-trained on ImageNet [Deng *et al.*, 2009] as the backbone. All the input images are data augmented with a sequence of being resized to the size of  $3 \times 384 \times 192$ , random horizontal flipping, and random channel erasing [Ye *et al.*, 2021]. The size of a mini-batch is set to 32, where we randomly sample 4 identities for each modality and 4 images for each identity. Besides, we adopt SGD as the optimizer with a weight decay of  $5 \times 10^{-4}$ , a momentum of 0.9, and a dynamic learning rate schedule, where the rate linearly increases from 0 to 0.1 in the first 10 epochs and de-



Method	Visible2Infrared		Infrared2Visible	
	Rank-1	mAP	Rank-1	mAP
Zero-Padding	17.75	18.90	16.63	17.82
D <sup>2</sup> RL	43.40	44.10	-	-
AlignGAN	57.90	53.60	56.30	53.40
Hi-CMD	70.93	66.04	-	-
cm-SSFT	72.30	72.90	71.00	71.70
DDAG	69.34	63.46	68.06	61.80
X-Modality	62.20	60.20	-	-
MMN	91.6	84.1	87.5	80.5
MPANet	82.8	80.7	83.7	80.9
LbA	67.64	74.17	65.46	72.43
MSA	84.86	82.16	-	-
JCCL	78.8	69.4	77.9	69.4
DCLNet	81.2	74.3	78.0	70.6
FMCNet	<b>89.12</b>	<b>84.43</b>	<b>88.38</b>	<b>83.86</b>
MAUM	87.87	85.09	86.95	84.34
CMM	59.81	60.86	-	-
SMCL	83.93	79.83	83.05	78.57
MID	87.45	84.85	84.29	81.41
PMCM(ours)	<b>93.09</b>	<b>89.57</b>	<b>91.44</b>	<b>87.15</b>

Table 2: Comparison of CMC and mAP performances with the SOTAs on RegDB.

creases by 0.1 per 30 epochs after the 30th epoch. The total number of training epochs is set to 101 and the number of tests is 10. In terms of hyper-parameters, we set  $\lambda_1$ ,  $\lambda_2$  and  $\lambda_3$  to 0.2, 0.2 and 1.0. Following [Hermans *et al.*, 2017], we set the margin of triplet loss to 0.3. The ratio  $p$  of patch-mix is set to 0.1 for SYSU-MM01 and 0.5 for RegDB. The parameter  $\mu$  is gradually increased to 0.5 in the first 50 rounds and kept until the end.

## 4.2 Comparison with State-of-the-Art Methods

We compare the proposed PMCM with several state-of-the-art methods for VI-ReID, including Zero-Padding [Wu *et al.*, 2017a], cmGAN [Dai *et al.*, 2018], D<sup>2</sup>RL [Wang *et al.*, 2019b], AlignGAN [Wang *et al.*, 2019a], Hi-CMD [Choi *et al.*, 2020], cm-SSFT [Lu *et al.*, 2020], CMM [Ling *et al.*, 2020], DDAG [Ye *et al.*, 2020b], X-Modality [Li *et al.*, 2020], MACE [Ye *et al.*, 2020a], MMN [Zhang *et al.*, 2021], MPANet [Wu *et al.*, 2021], LbA [Park *et al.*, 2021], SMCL [Wei *et al.*, 2021], MSA [Miao *et al.*, 2021], JCCL [Zhao *et al.*, 2021], DCLNet [Sun *et al.*, 2022], FMCNet [Zhang *et al.*, 2022], MAUM [Liu *et al.*, 2022b], and MID [Huang *et al.*, 2022].

The comparison results on SYSU-MM01 are shown in Table 1. We observe that our PMCM outperforms existing SOTAs on all evaluation metrics by a large margin. Specifically, PMCM achieves the Rank-1 accuracy of 75.54% and mAP of 71.16% in all-search and single-shot mode, respectively exceeding the second-best method MAMU by 3.68% and 2.37% points. Besides, we compared our method with other intermediate modality-based methods in the last four lines. We observe that our method outperforms the mixup-

Method	Rank-1	Rank-10	Rank-20	mAP
baseline	64.58	93.58	97.67	62.41
+Part	67.24	94.70	98.38	64.90
+PartAlign	69.52	95.98	98.82	65.37
+C2C	70.66	96.22	98.97	66.06
+PatchMix	73.76	97.34	99.22	69.88
+PMML	75.54	97.49	99.30	71.16

Table 3: Ablation studies on the effectiveness of each component of the proposed PMCM in SYSU-MM01.

Method	Rank-1	Rank-10	mAP
Grayscale	70.94	95.95	65.84
Mixup+PMML	73.26	96.95	69.39
PatchMix+PMML	<b>75.54</b>	<b>97.49</b>	<b>71.16</b>

Table 4: Comparison of different intermediate modality generation strategies on SYSU-MM01.

based method SMCL by 8.15% and 9.38%.

The comparison results on RegDB are shown in Table 2, where we obtain the best performance among the compared methods with rank-1 = 93.09% and mAP = 89.57% in Visible2Infrared mode and rank-1 = 91.44% and mAP = 87.15% in Infrared2Visible mode. Specifically, PMCM outperforms the second-best method FMCNet by 3.93% and 5.14% in Rank-1 and mAP in Visible2Infrared mode and 3.06% and 3.29% in Infrared2Visible mode. The consistent improvement in the two datasets demonstrate the superiority of our method, where more modality-invariant and discriminative features can be learned.

## 4.3 Ablation studies

To validate each component of PMCM, we conduct ablation experiments on SYSU-MM01 in the all-search and single-shot mode. The experimental result is shown in Table 3.

**Effectiveness of the part-based baseline (Part).** When exploring part features upon the global-based baseline, the performance is increased by 2.66% and 2.49% on Rank-1 and mAP, respectively, showing its enhancement to the feature representation learning.

**Effectiveness of the part alignment loss (PartAlign).** The part alignment loss plays the role of regularization to the global and part feature predictions. We observe that the improvements on Rank-1 accuracy and mAP are 2.32% and 0.47%, proving the part alignment loss better mines discriminative part features.

**Effectiveness of the center-to-center loss (C2C).** Compared with baseline, C2C improves the Rank-1 accuracy and mAP by 1.14% and 0.69%, thanks to that C2C pulls close the centers of different modalities of the same identity to extract modality-invariant features.

**Effectiveness of training with patch-mixed images (PatchMix).** As shown in the row '+PatchMix' in Table 3, after adding patch-mixed images for training, the Rank-1 accuracy and mAP are respectively increased by 3.10% and 3.82%, illustrating its effective. In addition, to show the

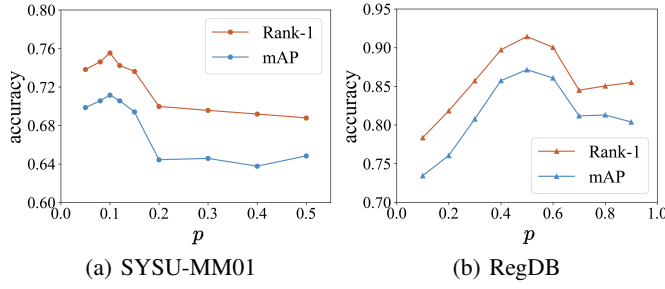


Figure 4: Influence of the different values of patch-mix ratio  $p$ , (a) is experiments on SYSU-MM01 in all-search and single-shot mode, and (b) is experiments on RegDB in Infrared2Visible mode.

size	Rank-1	Rank-10	Rank-20	mAP
$4 \times 4$	74.47	97.38	99.30	69.92
$8 \times 8$	75.09	97.27	99.26	70.93
$12 \times 12$	75.13	97.31	99.27	70.86
$16 \times 16$	<b>75.54</b>	<b>97.49</b>	<b>99.30</b>	<b>71.16</b>
$32 \times 32$	74.62	97.13	99.11	69.92

Table 5: Influence of different sizes of patch experimented in SYSU-MM01.

superiority of our method over other intermediate modality generation strategies, we compare images generated by grayscale and the standard mixup with PMML. As shown in Table 4, our method exceeds mixup by 2.28% and 1.77% on Rank-1 accuracy and mAP respectively. We also outperform the grayscale scheme by 4.60% and 5.28% on the two metrics. This fully demonstrates the advantage of our patch-mix scheme over other existing methods.

**Effectiveness of patch-mixed cross-modality learning (PMML).** The row '+PMML' in Table 3 provides sufficient evidence that PMML can further align between mixed modality and the two modalities, with its improvement to the Rank-1 accuracy and mAP by 1.78% and 1.28%.

#### 4.4 Algorithm Analysis

**Analysis of patch-mix ratio.** The ratio  $p$  adjusts the proportion of IR patches and RGB patches in the patch-mixed images. When  $p$  is 0, the image is composed of only an IR image. As  $p$  increases, more RGB patches are contained. As shown in Fig. 4, we evaluate the ratio  $p$  on both SYSU-MM01 in all-search single-shot mode and RegDB in Infrared2Visible mode.

On SYSU-MM01, the samples of IR modality are much fewer than that of RGB modality. We observe that when the ratio  $p$  is set to 0.5 (the number patches of two modalities are equal), a relatively low re-ID performance is obtained. When  $p$  decreases from 0.5 to 0.1 (more IR patches contained), the performance is continuously improved, and when the ratio is set to 1, the best performance is achieved. This demonstrate that, when there are more IR information contained in the intermediate modality, a better balance of IR and RGB data is kept, and model could learn the two modalities equally.

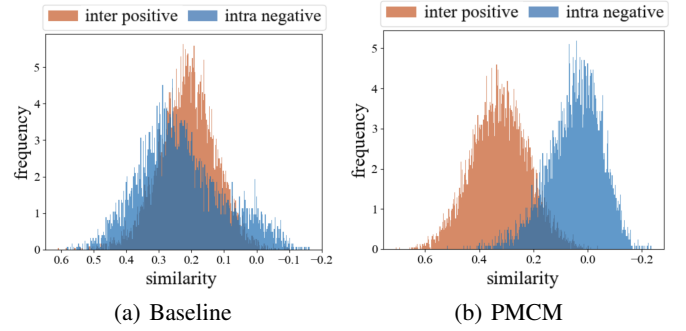


Figure 5: Visualization of cosine similarity distribution of inter-modality positive samples and intra-modality negative samples with (a) baseline and (b) our PMCM on the test set of SYSU-MM01.

On RegDB, IR and RGB modalities have the same number of samples, which means RegDB is a data-balanced dataset. As shown in Fig. 4 (b), the model achieves best performance when  $p$  is set to 0.5. In addition, when ratio is larger or smaller than 0.5, the balance between two modalities are broken, thus leading to performance decrease.

All evidences above prove that the proposed patch-mix scheme effectively alleviates the modality imbalance problem.

**Analysis of different sizes of the patch.** We conduct experiments to investigate the impact of different sizes of the image patches. As shown in Table 5, the patch size of  $4 \times 4$ ,  $8 \times 8$ ,  $12 \times 12$ ,  $16 \times 16$  and  $32 \times 32$  are explored. We observe that although both too large or too small sizes will slightly reduce the effect, our method is quite robust to the patch size. Finally, we choose the patch size of  $16 \times 16$  for our method.

#### 4.5 Visualization

As is shown in Fig. 5, we visualize the cosine distance distribution of inter-modality positive samples and intra-modality negative samples in the test set of SYSU-MM01. In baseline, the two types of image pair share a similar distance distributions, which reveals that the baseline can hardly retrieve inter-modality positive images. Instead, our proposed PMCM obviously separates the inter-positive pairs and intra-negative pairs, showing that cross-modality images could have bigger similarity and be retrieved successfully.

### 5 Conclusion

In this paper, we propose a Patch-Mixed Cross-Modality (PMCM) framework for VI-ReID. A patch-mixed modality is introduced to learn the correspondence between visible and infrared images and alleviate the modality imbalance problem. To further reduce the inter- and intra-modality variance, we propose a center-to-center loss to align the centers of the same identity from different modalities, and a part-alignment loss to constrain the consistency of part and global features. Extensive experiment results have demonstrated the superior effectiveness of PMCM compared with other state-of-the-art methods. The code will be publicly available, which would enable future researches.

## References

- [Cao *et al.*, 2019] Kaidi Cao, Colin Wei, Adrien Gaidon, Nikos Arechiga, and Tengyu Ma. Learning imbalanced datasets with label-distribution-aware margin loss. *Advances in neural information processing systems*, 32, 2019.
- [Choi *et al.*, 2020] Seokeon Choi, Sumin Lee, Youngeun Kim, Taekyung Kim, and Changick Kim. Hi-cmd: Hierarchical cross-modality disentanglement for visible-infrared person re-identification. In *CVPR*, pages 10257–10266, 2020.
- [Cui *et al.*, 2019] Yin Cui, Menglin Jia, Tsung-Yi Lin, Yang Song, and Serge Belongie. Class-balanced loss based on effective number of samples. In *CVPR*, pages 9268–9277, 2019.
- [Dai *et al.*, 2018] Pingyang Dai, Rongrong Ji, Haibin Wang, Qiong Wu, and Yuyu Huang. Cross-modality person re-identification with generative adversarial training. In *IJ-CAI*, volume 1, page 6, 2018.
- [Deng *et al.*, 2009] Jia Deng, Wei Dong, Richard Socher, Li-Jia Li, Kai Li, and Li Fei-Fei. Imagenet: A large-scale hierarchical image database. In *CVPR*, pages 248–255. Ieee, 2009.
- [Hermans *et al.*, 2017] Alexander Hermans, Lucas Beyer, and Bastian Leibe. In defense of the triplet loss for person re-identification. *arXiv preprint arXiv:1703.07737*, 2017.
- [Huang *et al.*, 2016] Chen Huang, Yining Li, Chen Change Loy, and Xiaoou Tang. Learning deep representation for imbalanced classification. In *CVPR*, pages 5375–5384, 2016.
- [Huang *et al.*, 2022] Zhipeng Huang, Jiawei Liu, Liang Li, Kecheng Zheng, and Zheng-Jun Zha. Modality-adaptive mixup and invariant decomposition for rgb-infrared person re-identification. *arXiv preprint arXiv:2203.01735*, 2022.
- [Li *et al.*, 2020] Diangang Li, Xing Wei, Xiaopeng Hong, and Yihong Gong. Infrared-visible cross-modal person re-identification with an x modality. In *AAAI*, volume 34, pages 4610–4617, 2020.
- [Ling *et al.*, 2020] Yongguo Ling, Zhun Zhong, Zhiming Luo, Paolo Rota, Shaozi Li, and Nicu Sebe. Class-aware modality mix and center-guided metric learning for visible-thermal person re-identification. In *ACMMM*, pages 889–897, 2020.
- [Ling *et al.*, 2021] Yongguo Ling, Zhiming Luo, Yaojin Lin, and Shaozi Li. A multi-constraint similarity learning with adaptive weighting for visible-thermal person re-identification. In *IJCAI*, pages 845–851, 2021.
- [Liu *et al.*, 2022a] Jialun Liu, Yifan Sun, Feng Zhu, Hongbin Pei, Yi Yang, and Wenhui Li. Learning memory-augmented unidirectional metrics for cross-modality person re-identification. In *CVPR*, pages 19366–19375, 2022.
- [Liu *et al.*, 2022b] Jialun Liu, Yifan Sun, Feng Zhu, Hongbin Pei, Yi Yang, and Wenhui Li. Learning memory-augmented unidirectional metrics for cross-modality person re-identification. In *CVPR*, pages 19366–19375, 2022.
- [Lu *et al.*, 2020] Yan Lu, Yue Wu, Bin Liu, Tianzhu Zhang, Baopu Li, Qi Chu, and Nenghai Yu. Cross-modality person re-identification with shared-specific feature transfer. In *CVPR*, pages 13379–13389, 2020.
- [Miao *et al.*, 2021] Ziling Miao, Hong Liu, Wei Shi, Wanlu Xu, and Hanrong Ye. Modality-aware style adaptation for rgb-infrared person re-identification. In *IJCAI*, pages 916–922, 2021.
- [Nguyen *et al.*, 2017] Dat Tien Nguyen, Hyung Gil Hong, Ki Wan Kim, and Kang Ryoung Park. Person recognition system based on a combination of body images from visible light and thermal cameras. *Sensors*, 17(3):605, 2017.
- [Park *et al.*, 2021] Hyunjong Park, Sanghoon Lee, Junghyup Lee, and Bumsub Ham. Learning by aligning: Visible-infrared person re-identification using cross-modal correspondences. In *ICCV*, pages 12046–12055, 2021.
- [Shen *et al.*, 2016] Li Shen, Zhouchen Lin, and Qingming Huang. Relay backpropagation for effective learning of deep convolutional neural networks. In *ECCV*, pages 467–482, 2016.
- [Sun *et al.*, 2018] Yifan Sun, Liang Zheng, Yi Yang, Qi Tian, and Shengjin Wang. Beyond part models: Person retrieval with refined part pooling (and a strong convolutional baseline). In *ECCV*, pages 480–496, 2018.
- [Sun *et al.*, 2022] Hanzhe Sun, Jun Liu, Zhizhong Zhang, Chengjie Wang, Yanyun Qu, Yuan Xie, and Lizhuang Ma. Not all pixels are matched: Dense contrastive learning for cross-modality person re-identification. In *ACMMM*, pages 5333–5341, 2022.
- [Wang *et al.*, 2019a] Guan’an Wang, Tianzhu Zhang, Jian Cheng, Si Liu, Yang Yang, and Zengguang Hou. Rgb-infrared cross-modality person re-identification via joint pixel and feature alignment. In *ICCV*, pages 3623–3632, 2019.
- [Wang *et al.*, 2019b] Zhixiang Wang, Zheng Wang, Yinqiang Zheng, Yung-Yu Chuang, and Shin’ichi Satoh. Learning to reduce dual-level discrepancy for infrared-visible person re-identification. In *CVPR*, pages 618–626, 2019.
- [Wei *et al.*, 2021] Ziyu Wei, Xi Yang, Nannan Wang, and Xinbo Gao. Syncretic modality collaborative learning for visible infrared person re-identification. In *ICCV*, pages 225–234, 2021.
- [Wu *et al.*, 2017a] Ancong Wu, Wei-Shi Zheng, Hong-Xing Yu, Shaogang Gong, and Jianhuang Lai. Rgb-infrared cross-modality person re-identification. In *ICCV*, pages 5380–5389, 2017.
- [Wu *et al.*, 2017b] Ancong Wu, Wei-Shi Zheng, Hong-Xing Yu, Shaogang Gong, and Jianhuang Lai. Rgb-infrared cross-modality person re-identification. In *ICCV*, pages 5380–5389, 2017.
- [Wu *et al.*, 2021] Qiong Wu, Pingyang Dai, Jie Chen, Chia-Wen Lin, Yongjian Wu, Feiyue Huang, Bineng Zhong, and



- Rongrong Ji. Discover cross-modality nuances for visible-infrared person re-identification. In *CVPR*, pages 4330–4339, 2021.
- [Ye *et al.*, 2018a] Mang Ye, Xiangyuan Lan, Jiawei Li, and Pong Yuen. Hierarchical discriminative learning for visible thermal person re-identification. In *AAAI*, volume 32, 2018.
- [Ye *et al.*, 2018b] Mang Ye, Zheng Wang, Xiangyuan Lan, and Pong C Yuen. Visible thermal person re-identification via dual-constrained top-ranking. In *IJCAI*, volume 1, page 2, 2018.
- [Ye *et al.*, 2020a] Mang Ye, Xiangyuan Lan, Qingming Leng, and Jianbing Shen. Cross-modality person re-identification via modality-aware collaborative ensemble learning. *IEEE Transactions on Image Processing*, 29:9387–9399, 2020.
- [Ye *et al.*, 2020b] Mang Ye, Jianbing Shen, David J Crandall, Ling Shao, and Jiebo Luo. Dynamic dual-attentive aggregation learning for visible-infrared person re-identification. In *ECCV*, pages 229–247, 2020.
- [Ye *et al.*, 2020c] Mang Ye, Jianbing Shen, and Ling Shao. Visible-infrared person re-identification via homogeneous augmented tri-modal learning. *IEEE Transactions on Information Forensics and Security*, 16:728–739, 2020.
- [Ye *et al.*, 2021] Mang Ye, Weijian Ruan, Bo Du, and Mike Zheng Shou. Channel augmented joint learning for visible-infrared recognition. In *ICCV*, pages 13567–13576, 2021.
- [Zhang *et al.*, 2017] Hongyi Zhang, Moustapha Cisse, Yann N Dauphin, and David Lopez-Paz. mixup: Beyond empirical risk minimization. *arXiv preprint arXiv:1710.09412*, 2017.
- [Zhang *et al.*, 2021] Yukang Zhang, Yan Yan, Yang Lu, and Hanzi Wang. Towards a unified middle modality learning for visible-infrared person re-identification. In *ACMMM*, pages 788–796, 2021.
- [Zhang *et al.*, 2022] Qiang Zhang, Changzhou Lai, Jianan Liu, Nianchang Huang, and Jungong Han. Fmcnet: Feature-level modality compensation for visible-infrared person re-identification. In *CVPR*, pages 7349–7358, 2022.
- [Zhao *et al.*, 2021] Zhiwei Zhao, Bin Liu, Qi Chu, Yan Lu, and Nenghai Yu. Joint color-irrelevant consistency learning and identity-aware modality adaptation for visible-infrared cross modality person re-identification. In *AAAI*, volume 35, pages 3520–3528, 2021.